Journal of Computational Physics 291 (2015) 303–316

Contents lists available at ScienceDirect

Journal of Computational Physics

www.elsevier.com/locate/jcp

Numerical scheme for a spatially inhomogeneous matrix-valued quantum Boltzmann equation ☆

Jianfeng Lu [a], Christian B. Mendl [b]

[a] Departments of Mathematics, Physics, and Chemistry, Duke University, Box 90320, Durham, NC 27708, USA
[b] Mathematics Department, Technische Universität München, Boltzmannstraße 3, 85747 Garching bei München, Germany

ARTICLE INFO

Article history:
Received 8 August 2014
Received in revised form 23 January 2015
Accepted 10 March 2015
Available online 18 March 2015

Keywords:
Quantum Boltzmann equation
Hubbard model
Fourier spectral method

ABSTRACT

We develop an efficient algorithm for a spatially inhomogeneous matrix-valued quantum Boltzmann equation derived from the Hubbard model. The distribution functions are 2×2 matrix-valued to accommodate the spin degree of freedom, and the scalar quantum Boltzmann equation is recovered as a special case when all matrices are proportional to the identity. We use Fourier discretization and fast Fourier transform to efficiently evaluate the collision kernel with spectral accuracy, and numerically investigate periodic, Dirichlet and Maxwell boundary conditions. Model simulations quantify the convergence to local and global thermal equilibrium.

1. Introduction

Boltzmann's kinetic theory is widely used to describe the dynamics of rarified gases. Immediately after the discovery of quantum mechanics, a modification of the classical Boltzmann equation to take quantum interactions into account has been proposed by Nordheim [12] (with a more systematic derivation by Peierls [13]), and by Uehling and Uhlenbeck [18,19]. With the inclusion of quantum mechanical effects into the collision operator, the quantum Boltzmann equation has many applications, e.g., for the kinetic description of Bose–Einstein condensation [15,16], spintronics and decoherence theory in quantum computing [2,14,20,22], or kinetic modeling of semiconductor devices [9].

In recent works, starting from the Hubbard model in the weak interaction limit, a matrix-valued Boltzmann equation has been derived [4–6] for the spatially homogeneous setting without advection term. To describe spatially inhomogeneous systems, one combines the Boltzmann transport equation with the collision term derived in [4]:

$$\partial_t W + v_x \partial_x W = \mathscr{C}[W] - i[\vec{B} \cdot \vec{\sigma}, W], \tag{1}$$

where the state variable W is the Wigner distribution of the spin-density matrix, $\vec{B}$ is an external magnetic field, $\vec{\sigma}$ are the Pauli matrices, and the collision term $\mathscr{C}[W]$ will be specified below in Section 2. We emphasize that while the form of the equation follows the usual quantum Boltzmann equation, the collision term is quite different (which is systematically derived from a many-body quantum mechanics model), and the matrix-valued W distinguishes the equation from the usual kinetic equations.

☆ We would like to thank Jingwei Hu, Lorenzo Pareschi and Herbert Spohn for helpful discussions. The work of J.L. was supported in part by the Alfred P. Sloan Foundation and the National Science Foundation under award DMS-1312659. C.M. would like to thank the warm hospitality of the Mathematics Department at Duke University where part of the work was done, as well as support from DFG under grant FR 1275/3-1.

E-mail addresses: jianfeng@math.duke.edu (J. Lu), mendl@ma.tum.de (C.B. Mendl).

http://dx.doi.org/10.1016/j.jcp.2015.03.020
0021-9991/

The focus of this paper is devising an efficient algorithm for solving (1). Our goal in this work is twofold: First, we would like to develop a numerical scheme that systematically converges to the true solution; for that purpose, we use a spectral method in the velocity variable. The collision operator, albeit much more complicated than for the usual classical or scalar quantum Boltzmann equation, can be efficiently calculated using Carleman representation and fast Fourier transforms. Second, we want to investigate non-trivial boundary conditions, like Dirichlet and Maxwell boundary conditions, and the effect of external magnetic fields. These developments should lead to a better understanding of the physics modeled by these equations.

Kinetic equations are traditionally solved by Monte Carlo methods (also known as particle methods). In recent years, the development of efficient real space or Fourier space methods to solve Boltzmann equations has been a very active research area. In particular, the line of research initiated by [11] and further developed in [3,7] is especially relevant for our approach. The paper [11] proposed a fast algorithm for computing the Boltzmann collision kernel based on Fourier discretization, and [7] further improved the efficiency of the algorithm. The method we develop in this work for the collision operator of the matrix-valued Boltzmann equation is closely related, albeit with some differences: (a) Since we are dealing with collision terms originating from quantum mechanics, the microscopic energy is not necessarily conserved (see the effective Hamiltonian in Eq. (6) below); some new ideas are required to treat the resulting terms. (b) To evaluate double convolutions exactly using fast Fourier transforms, we use a double padding approach to avoid aliasing issues. As a result, while maintaining the spectral accuracy, the scheme also nicely respects the conservation law of the continuous equation. Further details can be found in Section 3.

A numerical algorithm for the spatially homogeneous matrix-valued Boltzmann equation in one dimension was considered before in [5,6], which calculates the collision term directly using numerical quadrature. A subsequent work by one of the authors [10] considers a lattice Boltzmann method (LBM) for the spatially inhomogeneous equation with periodic boundary conditions, which can be understood as a discrete velocity method with very few velocity grid points. Due to the small number of grid points, the accuracy of the numerical result compared to the original equation is not guaranteed. In contrast to that, the method proposed here systematically approximates the original equation as we refine the grid.

Considering the *matrix-valued* Boltzmann equation, it is useful to represent the spin-density Wigner distribution in the basis of Pauli matrices. In fact, the formulas for the collision terms are more compact in the new representation, which might be of independent interest for understanding the physics and mathematics of the equation.

The rest of the paper is organized as follows. We introduce the spatially inhomogeneous matrix-valued Boltzmann equation and its associated boundary conditions in Section 2. We will focus on the development of the fast algorithm for the collision operator in Section 3. To deal with the spatial degree of freedom, we use the finite volume method and a parallel implementation based on MPI; this is discussed in Section 4. We show some numerical results for validating the algorithm and for exploring interesting physical phenomena in Section 5. Finally we wrap up the paper with some conclusive remarks in Section 6.

2. The spatially inhomogeneous matrix-valued Boltzmann equation

The starting point for the derivation [4] of the matrix-valued Boltzmann equation is the Hubbard model with a weak pair potential λV such that $0 < \lambda \ll 1$. Consider a spin-$\frac{1}{2}$ Fermi field with annihilation operators $a_s(x)$, $x \in \mathbb{Z}^d$, $s \in \{\uparrow, \downarrow\}$, obeying the anti-commutation relations

$$\left\{a_s(x)^\dagger, a_{s'}(x')\right\} = \delta_{xx'}\delta_{ss'}, \quad \left\{a_s(x), a_{s'}(x')\right\} = 0, \quad \text{and} \quad \left\{a_s(x)^\dagger, a_{s'}(x')^\dagger\right\} = 0,$$

where $A^\dagger$ denotes the adjoint operator of A. Using the second quantization formulation, the (many-body) Hamiltonian of the Hubbard system is then given by

$$H = \sum_{x,y\in\mathbb{Z}^d} \sum_{s\in\{\uparrow,\downarrow\}} \alpha(x-y) a_s(x)^\dagger a_s(y) + \frac{1}{2} \sum_{x\in\mathbb{Z}^d} \sum_{s,s'\in\{\uparrow,\downarrow\}} \lambda V(x-y) a_s(x)^\dagger a_s(x) a_{s'}(y)^\dagger a_{s'}(y). \tag{2}$$

Here the first term on the right hand side in the Hamiltonian describes the hopping from site y to x with α the hopping amplitude, and the non-quadratic second term gives the interactions of two excitons with V the interaction potential. The grid $\mathbb{Z}^d$ must be distinguished from the spatial dimension considered below (in some sense, the grid $\mathbb{Z}^d$ is on the microscopic scale while the spatial inhomogeneity is introduced on a mesoscopic scale). In Fourier representation, the time-dependent (Heisenberg picture) field operators $\hat{a}_s(t, v)$ adhere to the initial ($t = 0$) anti-commutation relation $\{\hat{a}_s(v)^\dagger, \hat{a}_{s'}(v')\} = \delta_{ss'}\delta(v - v')$, with v, v' denoting velocity variables. As discussed in [4], the time-dependent average Wigner matrix W defined by

$$\left\langle \hat{a}_s(t, v)^\dagger \hat{a}_{s'}(t, v') \right\rangle = \delta(v - v') W_{ss'}(t, v) \tag{3}$$

will approximately satisfy a Boltzmann kinetic equation $\partial_t W = \mathscr{C}[W]$ for times up to order λ^{-2}. Here, as in the Heisenberg picture, the average $\langle\cdot\rangle$ is taken with respect to the initial state of the system. The effective Boltzmann equation is much easier to solve compared to the original quantum many-body system, which is an extremely high-dimensional problem.

Augmenting the Boltzmann equation with the usual transport term for the spatially inhomogeneous setting and including an external magnetic field $\vec{B}$, one arrives at Eq. (1), where $\vec{\sigma} = (\sigma_1, \sigma_2, \sigma_3)$ are the Pauli matrices:

$$\sigma_1 = \begin{pmatrix} 0 & 1 \\ 1 & 0 \end{pmatrix}, \quad \sigma_2 = \begin{pmatrix} 0 & -i \\ i & 0 \end{pmatrix}, \quad \sigma_3 = \begin{pmatrix} 1 & 0 \\ 0 & -1 \end{pmatrix}. \tag{4}$$

Hence $\vec{B}\cdot\vec{\sigma} = \sum_{i=1}^{3} B_i\sigma_i$. In (1), the Hermitian spin-density matrix Wigner distribution $W : \mathbb{R}_+ \times \Omega \times \mathbb{R}^2 \to \mathbb{C}^{2\times 2}$ additionally depends on the spatial location $x \in \Omega$. When the system is spatially homogeneous, W as defined in (3) is a positive-semidefinite Hermitian matrix with eigenvalues in $[0, 1]$ at any (t, v). In the case of (1) where spatial inhomogeneity is introduced on a mesoscopic scale, we likewise assume that initially the Wigner matrix $W(0, x, v)$ is positive-semidefinite with eigenvalues in $[0, 1]$ at any (x, v). This property is preserved by the evolution of (3).

For simplicity, we will only consider the case that Ω is an open and bounded interval on $\mathbb{R}$; and assume that the velocity space is $\mathbb{R}^2$. In other words, we are considering the case with one space dimension and two velocity dimensions. Physically, this means that the solution is homogeneous with respect to one of the spatial variables for a full two-dimensional (two space and two velocity dimensions) model. Without loss of generality, we will also assume $\Omega = (0, 1)$.

The collision operator in (1) consists of a conservative and dissipative part: $\mathscr{C} = \mathscr{C}_c + \mathscr{C}_d$, where [5,6]

$$\mathscr{C}_c[W](t, x, v) = -i\big[H_{\text{eff}}(t, x, v), W(t, x, v)\big] \tag{5}$$

with the effective Hamiltonian

$$H_{\text{eff}}(t, x, v_1) = \int \mathrm{d}v_2\,\mathrm{d}v_3\,\mathrm{d}v_4\,\delta(\underline{v})\mathscr{P}(1/\underline{\omega})(W_3W_4 - W_2W_3 - W_3W_2 - \operatorname{tr}[W_4]W_3 + \operatorname{tr}[W_2]W_3 + W_2). \tag{6}$$

Here $\mathscr{P}$ denotes the principal value, and we have used the shorthand notations $W_i = W(t, x, v_i)$ for $i = 1, \ldots, 4$, the velocity difference $\underline{v} = v_1 + v_2 - v_3 - v_4$, and the energy difference $\underline{\omega} = \omega(v_1) + \omega(v_2) - \omega(v_3) - \omega(v_4)$. The energy (or dispersion relation) $\omega(v)$ is precisely the Fourier transform of the hopping amplitude α appearing in (2). The terms W_iW_j are usual matrix products. Due to the invariance under $v_3 \leftrightarrow v_4$, the matrix product W_3W_4 in the integrand could be replaced by W_4W_3; in particular, H_{eff} is Hermitian.

The dissipative part of the collision operator is given by

$$\mathscr{C}_d[W](t, x, v_1) = \pi \int \mathrm{d}v_2\,\mathrm{d}v_3\,\mathrm{d}v_4\delta(\underline{v})\delta(\underline{\omega})\big(\mathscr{A}[W]_{1234} + \mathscr{A}[W]^*_{1234}\big) \tag{7}$$

with

$$\begin{aligned}\mathscr{A}[W]_{1234} = &-W_4\tilde{W}_2W_3 + W_4\operatorname{tr}[\tilde{W}_2W_3] \\ &- \big(\tilde{W}_4W_3 - \tilde{W}_4W_2 - \tilde{W}_2W_3 + \tilde{W}_4\operatorname{tr}[W_2] - \tilde{W}_4\operatorname{tr}[W_3] + \operatorname{tr}[W_3\tilde{W}_2]\big)W_1,\end{aligned} \tag{8}$$

where $\tilde{W} = \mathbb{1} - W$. As explained in [5,6], the first two summands (plus their Hermitian conjugates) can be identified as gain term and $(\ldots)W_1$ (plus Hermitian conjugate) as loss term. Alternatively, by making use of the invariance under $v_3 \leftrightarrow v_4$, the integrand of $\mathscr{C}_d[W]$ can be represented as

$$\mathscr{A}[W]_{1234} + \mathscr{A}[W]^*_{1234} \equiv \mathscr{A}_{\text{quad}}[W]_{1234} + \mathscr{A}_{\text{tr}}[W]_{1234} \tag{9}$$

with

$$\begin{aligned}\mathscr{A}_{\text{quad}}[W]_{1234} &= -\tilde{W}_1W_3\tilde{W}_2W_4 - W_4\tilde{W}_2W_3\tilde{W}_1 + W_1\tilde{W}_3W_2\tilde{W}_4 + \tilde{W}_4W_2\tilde{W}_3W_1, \\ \mathscr{A}_{\text{tr}}[W]_{1234} &= \big(\tilde{W}_1W_3 + W_3\tilde{W}_1\big)\operatorname{tr}[\tilde{W}_2W_4] - \big(W_1\tilde{W}_3 + \tilde{W}_3W_1\big)\operatorname{tr}[W_2\tilde{W}_4].\end{aligned} \tag{10}$$

The representation (10) emphasizes the similarity to the scalar collision operator [19], which is recovered when all W_i are proportional to the identity matrix. For what follows, we always take $\omega(v) = \frac{1}{2}|v|^2$ as dispersion relation. Note that if a general dispersion relation is taken, the transport term in (1) changes to $(\partial_{v_x}\omega(v))\cdot\partial_x W$.

One may check that the collision operator $\mathscr{C} = \mathscr{C}_c + \mathscr{C}_d$ satisfies the density, momentum and energy conservation laws (at each x)

$$\int \mathscr{C}[W](v)\,\mathrm{d}v = 0, \quad \int v\operatorname{tr}\big[\mathscr{C}[W](v)\big]\,\mathrm{d}v = 0, \quad \int \tfrac{1}{2}|v|^2\operatorname{tr}\big[\mathscr{C}[W](v)\big]\,\mathrm{d}v = 0. \tag{11}$$

As a result, the corresponding fluid dynamic moments, i.e., density $\rho(t, x) \in \mathbb{C}^{2\times 2}$, velocity $u(t, x) \in \mathbb{R}^2$, and internal energy $\varepsilon(t, x) \in \mathbb{R}$

$$\rho(t, x) = \int W(t, x, v)\,\mathrm{d}v; \tag{12}$$

$$\operatorname{tr}[\rho(t, x)]u(t, x) = \int v\operatorname{tr}[W(t, x, v)]\,\mathrm{d}v; \tag{13}$$

$$\operatorname{tr}[\rho(t, x)]\varepsilon(t, x) = \int \tfrac{1}{2}|v - u|^2\operatorname{tr}[W(t, x, v)]\,\mathrm{d}v \tag{14}$$

satisfy local conservation laws.

The (local) entropy of the state W is defined as

$$S[W](t,x) = -\int \mathrm{tr}\big[W(t,x,v)\log W(t,x,v) + \tilde{W}(t,x,v)\log\tilde{W}(t,x,v)\big]\,\mathrm{d}v. \tag{15}$$

The H-theorem states that the global entropy production rate is positive (see [5] for the matrix-valued case)

$$\sigma[W](t) := \frac{\mathrm{d}}{\mathrm{d}t}\int S[W](t,x)\,\mathrm{d}x = -\int\int \mathrm{tr}\Big[\big(\log W(t,x,v) - \log\tilde{W}(t,x,v)\big)\mathscr{C}[W](t,x,v)\Big]\,\mathrm{d}v\,\mathrm{d}x \geq 0 \tag{16}$$

for all W with eigenvalues in $[0,1]$ and periodic boundary conditions. The advection term in the integrand vanishes since we integrate over the spatial domain.

In the asymptotic long-time limit $t\to\infty$ for a closed system (with periodic boundary conditions) and in the absence of external fields, the solution of the Boltzmann equation (1) is expected to converge to the Fermi–Dirac distribution

$$W_{\mathrm{FD}}(v) = \sum_{s\in\{\uparrow,\downarrow\}} \big(\mathrm{e}^{(\omega(v)-\mu_s)/(k_{\mathrm{B}}T)}+1\big)^{-1}|s\rangle\langle s| \tag{17}$$

for a v-independent spin basis $|s\rangle$, temperature T, and chemical potentials $\mu_\uparrow$ and $\mu_\downarrow$ (see [5] for a proof of convergence in the spatially homogeneous case). Note that the Fermi–Dirac distribution maximizes the entropy among states with the same fluid dynamic moments. The moments of W_{FD} have analytical expressions: in two dimensions and for the dispersion $\omega(v) = \frac{1}{2}|v|^2$,

$$\rho_{\mathrm{FD}} = 2\pi k_{\mathrm{B}}T\sum_{s\in\{\uparrow,\downarrow\}}\log\big(1+\mathrm{e}^{\mu_s/(k_{\mathrm{B}}T)}\big),\quad \varepsilon_{\mathrm{FD}} = k_{\mathrm{B}}T\frac{-\sum_{s\in\{\uparrow,\downarrow\}}\mathrm{Li}_2\big(-\mathrm{e}^{\mu_s/(k_{\mathrm{B}}T)}\big)}{\sum_{s\in\{\uparrow,\downarrow\}}\log\big(1+\mathrm{e}^{\mu_s/(k_{\mathrm{B}}T)}\big)} \tag{18}$$

where Li_n is the polylogarithm function. The average velocity of W_{FD} in (17) is zero.

To complete the equation, we need to impose the boundary conditions. Let $\Sigma = \partial\Omega\times\mathbb{R}^2 = \{0,1\}\times\mathbb{R}^2$, and denote by $n(x)$ be the outward unit normal vector at $x\in\partial\Omega$. We define the outgoing and incoming boundaries as

$$\Sigma_\pm = \big\{(x,v)\in\Sigma;\ \pm n(x)\cdot v > 0\big\}. \tag{19}$$

Hence

$$\Sigma_+ = \big\{(0,v);\ v_x<0\big\}\cup\big\{(1,v);\ v_x>0\big\}; \tag{20}$$

$$\Sigma_- = \big\{(0,v);\ v_x>0\big\}\cup\big\{(1,v);\ v_x<0\big\}. \tag{21}$$

For the boundary condition on the incoming boundary Σ_-, we consider

- periodic boundary conditions: for $(x,v)\in\Sigma_-$,
$$W(t,x,v) = W(t,1-x,v). \tag{22}$$
Note that $(1-x,v)\in\Sigma_+$.
- Dirichlet boundary conditions: for $(x,v)\in\Sigma_-$,
$$W(t,x,v) = \Phi(t,x,v) \tag{23}$$
where $\Phi:\mathbb{R}_+\times\Sigma_-\to\mathbb{C}^{2\times2}$ is a given boundary state.
- Maxwell boundary conditions:
$$W(t,x,v) = \mathscr{R}_x\big(W(t,x,\cdot)|_{\Sigma_+^x}\big)(v), \tag{24}$$
where $\mathscr{R}_x$ is a Maxwell reflection operator:
$$\mathscr{R}_x = (1-\alpha)\mathscr{L}_x + \alpha\mathscr{D}_x. \tag{25}$$
Here $\alpha\in[0,1]$ is the accommodation coefficient. The local reflection operator $\mathscr{L}_x$ is given by
$$\big(\mathscr{L}_xF\big)(v_x,v_y) = F(-v_x,v_y), \tag{26}$$
and the diffusive reflection is given by (for a specified Fermi–Dirac state depending on spin basis, T, $\mu_\uparrow$ and $\mu_\downarrow$)
$$(\mathscr{D}_xF)(v) = Z_x^{-1}W_{\mathrm{FD}}(v)\overline{F}(x), \tag{27}$$
where $\overline{F}(x)$ is the total outgoing number flux
$$\overline{F}(x) = \int_{v\cdot n(x)>0}\mathrm{tr}(F(v))v\cdot n(x)\,\mathrm{d}v, \tag{28}$$
and Z_x is a normalizing constant such that
$$Z_x = \int_{v\cdot n(x)<0}\mathrm{tr}(W_{\mathrm{FD}}(v))|v\cdot n(x)|\,\mathrm{d}v. \tag{29}$$

In the following, we introduce an efficient and accurate numerical scheme for the Boltzmann equation (1).

3. Fast spectral method for the collision operator

Calculating the collision operator is the computationally most demanding step in solving (1). Here, we first represent the collision operator using Pauli matrices, and then develop a fast Fourier spectral method inspired by the ideas in [3,7,11].

3.1. Representation of the collision operator using Pauli matrices

Since the spin-density matrix $W(t,x,v)$ is Hermitian, it can be represented in the basis of the identity matrix and the Pauli matrices:

$$W_i = W(v_i) = w_{i,0}\mathbb{1} + \sum_{j=1}^{3} w_{i,j}\sigma_j, \tag{30}$$

where the subscript i specifies the velocity dependence, and we have suppressed the dependence on (t,x) for concise notation. Moreover, we define the vector of components as

$$w_i = (w_{i,0}, w_{i,1}, w_{i,2}, w_{i,3}) \in \mathbb{R}^4, \tag{31}$$

and introduce the notation $\boldsymbol{\sigma} = (\mathbb{1}, \vec{\sigma})$ so that

$$w_i \cdot \boldsymbol{\sigma} = w_{i,0}\mathbb{1} + \sum_{j=1}^{3} w_{i,j}\sigma_j. \tag{32}$$

The 3-vector part $\vec{w}_i = (w_{i,1}, w_{i,2}, w_{i,3}) \in \mathbb{R}^3$ is exactly the Bloch vector of W_i (up to normalization), and the eigenvalues of W_i are $w_{i,0} \pm |\vec{w}_i|$.

We will also use the 4×4 "metric tensor" $\eta = \mathrm{diag}(1,-1,-1,-1)$ and set

$$\langle w_i, w_j\rangle_\eta = w_i^T \eta\, w_j. \tag{33}$$

Since the eigenvalues of W_i are in the interval $[0,1]$, one can verify that likewise $\langle w_i, w_j\rangle_\eta \in [0,1]$.

Using the interchangeability of $v_3 \leftrightarrow v_4$ in the integral, the gain term of the dissipative collision operator (7) can be written as

$$-W_4\tilde{W}_2W_3 + W_4\,\mathrm{tr}[\tilde{W}_2W_3] + \mathrm{h.c.} \equiv 2\langle w_3, w_4\rangle_\eta\big(\mathbb{1} - (\eta\, w_2)\cdot\boldsymbol{\sigma}\big), \tag{34}$$

and the loss term as

$$\begin{aligned}&-\big(\tilde{W}_4W_3 - \tilde{W}_4W_2 - \tilde{W}_2W_3 + \tilde{W}_4\,\mathrm{tr}[W_2] - \tilde{W}_4\,\mathrm{tr}[W_3] + \mathrm{tr}[W_3\tilde{W}_2]\big)W_1 + \mathrm{h.c.}\\ &\quad\equiv -\big(\langle w_3, w_4\rangle_\eta\mathbb{1} - (w_{3,0} + w_{4,0} - 1)\,(\eta\, w_2)\cdot\boldsymbol{\sigma}\big)W_1 + \mathrm{h.c.}\end{aligned} \tag{35}$$

For the Hermitian conjugate, one requires the anti-commutator of two Wigner matrices, which reads in the Pauli representation

$$\big\{W_1, W_2\big\} \equiv W_1W_2 + W_2W_1 = 2\big((w_{1,0}w_2 + w_{2,0}w_1)\cdot\boldsymbol{\sigma} - \langle w_1, w_2\rangle_\eta\mathbb{1}\big). \tag{36}$$

Again using the interchangeability of $v_3 \leftrightarrow v_4$ in the integral, the integrand in Eq. (6) of the conservative collision operator (5) becomes

$$\begin{aligned}&(W_3W_4 - W_2W_3 - W_3W_2 - \mathrm{tr}[W_4]W_3 + \mathrm{tr}[W_2]W_3 + W_2)\\ &\quad\equiv \big(\langle w_2, w_2\rangle_\eta - \langle w_3 - w_2, w_4 - w_2\rangle_\eta\big)\mathbb{1} - (w_{3,0} + w_{4,0} - 1)W_2.\end{aligned} \tag{37}$$

Since the identity matrix does not contribute to the commutator in Eq. (5), it suffices to keep the second term $-(w_{3,0} + w_{4,0} - 1)W_2$ only. The commutator in Eq. (5) reads in the Pauli matrix representation

$$-i\big[W_2, W_1\big] = 2\,(\vec{w}_2 \times \vec{w}_1)\cdot\vec{\sigma}. \tag{38}$$

To summarize, we have obtained the representation

$$\mathscr{C}_{\mathrm{c}}[W]_1 = i\int \mathrm{d}v_2\,\mathrm{d}v_3\,\mathrm{d}v_4\,\delta(\underline{v})\mathscr{P}(1/\underline{\omega})(w_{3,0} + w_{4,0} - 1)\big[W_2, W_1\big], \tag{39}$$

and similarly

$$\begin{aligned}\mathscr{C}_{\mathrm{d}}[W]_1 = \pi\int \mathrm{d}v_2\,\mathrm{d}v_3\,\mathrm{d}v_4\,\delta(\underline{v})\delta(\underline{\omega})\Big(&2\langle w_3, w_4\rangle_\eta\big(\mathbb{1} - W_1 - (\eta w_2)\cdot\boldsymbol{\sigma}\big)\\ &+ (w_{3,0} + w_{4,0} - 1)\big\{W_1, (\eta w_2)\cdot\boldsymbol{\sigma}\big\}\Big).\end{aligned} \tag{40}$$

We remark that it is also possible to write the matrix-valued Boltzmann equation as a kinetic equation with multiple components, if we regard each matrix entry as a component. However, we prefer the more natural and physical representation in terms of Pauli matrices.

3.2. Fast Fourier spectral method

To efficiently evaluate the collision terms (39) and (40), we generalize the ideas in [3,7,11] for a Fourier spectral discretization of the velocity space.

Let us discuss the conservative part (39) first. Using the Carleman representation [1,21], we perform a change of variables $v_1 \mapsto v$, $v_3 \mapsto v+u$, $v_4 \mapsto v+u'$, such that

$$v_2 = v_3 + v_4 - v_1 = v + u + u';$$
$$\underline{\omega} = \omega(v_1) + \omega(v_2) - \omega(v_3) - \omega(v_4) = u \cdot u'.$$

Substituting into (39), we arrive at

$$\mathscr{C}_c[W](v) = i \int_{B_R} \int_{B_R} \mathrm{d}u\, \mathrm{d}u'\, \mathscr{P}(1/(u\cdot u'))(2w_0(v+u)-1)\big(W(v+u+u')W(v) - \text{h.c.}\big), \tag{41}$$

where we have used the symmetry between u and u'. Here R indicates the truncation of the collision integral, taken so that B_R approximately covers the support of W in the v variable. Hence, we just need to deal with integrals of the kind

$$I_1(v) = \int_{B_R} \int_{B_R} \mathrm{d}u\, \mathrm{d}u'\, \mathscr{P}(1/(u\cdot u'))\, f(v+u) g(v+u+u') h(v). \tag{42}$$

To apply the Fourier method, we periodize the functions f, g and h etc. on the domain $[-L,L]^2$ with $L \geq \frac{3+\sqrt{2}}{2}R$, and define the Fourier grid

$$\Xi = [-N/2, -N/2+1, \ldots, N/2-1]^2. \tag{43}$$

Here the cut-off frequency N controls the accuracy. Using the Fourier inversion formula, we approximate

$$f(v) \approx \sum_{\xi\in\Xi} \widehat{f}(\xi) \exp(i\pi\xi\cdot v/L) \quad \text{and} \quad \widehat{f}(\xi) = \fint_{[-L,L]^2} f(v) \mathrm{e}^{-i\frac{\pi}{L}\xi\cdot v}\, \mathrm{d}v \tag{44}$$

Then

$$\begin{aligned} I_1(v) &= \sum_{\chi,\eta,\zeta} \int_{B_R}\int_{B_R} \mathrm{d}u\, \mathrm{d}u'\, \mathscr{P}(1/(u\cdot u'))\widehat{f}(\chi)\widehat{g}(\eta)\widehat{h}(\zeta) \mathrm{e}^{i\frac{\pi}{L}v\cdot(\chi+\eta+\zeta)} \mathrm{e}^{i\frac{\pi}{L}u\cdot(\chi+\eta)} \mathrm{e}^{i\frac{\pi}{L}u'\cdot\eta} \\ &= \sum_{\chi,\eta,\zeta} \widehat{f}(\chi)\widehat{g}(\eta)\widehat{h}(\zeta) \mathrm{e}^{i\frac{\pi}{L}v\cdot(\chi+\eta+\zeta)} G(\chi+\eta,\eta) \end{aligned} \tag{45}$$

where the matrix $G(\xi,\chi)$ is defined as

$$G(\xi,\chi) = \int_{B_R} \mathrm{d}u \int_{B_R} \mathrm{d}u'\, \mathscr{P}(1/(u\cdot u')) \exp(i\pi\xi\cdot u/L) \exp(i\pi\chi\cdot u'/L). \tag{46}$$

Changing to polar coordinates, one obtains

$$G(\xi,\chi) = \int_0^R \mathrm{d}r \int_0^R \mathrm{d}r' \int_{S^1} \mathrm{d}\theta \int_{S^1} \mathrm{d}\theta'\, \mathscr{P}\big(1/(\theta\cdot\theta')\big) \exp\big(i\pi\xi\cdot\theta r/L\big) \exp\big(i\pi\chi\cdot\theta' r'/L\big). \tag{47}$$

Since $\mathscr{P}(1/(\theta\cdot\theta'))$ is odd in both θ and θ', it suffices to take the odd part of the complex exponentials in the above integral, and we get

$$G(\xi,\chi) = -\int_0^R \mathrm{d}r \int_0^R \mathrm{d}r' \int_{S^1} \mathrm{d}\theta \int_{S^1} \mathrm{d}\theta'\, \mathscr{P}\big(1/(\theta\cdot\theta')\big) \sin\big(\pi\xi\cdot\theta r/L\big) \sin\big(\pi\chi\cdot\theta' r'/L\big). \tag{48}$$

Note that

$$\phi_R(\xi\cdot\theta) = \int_0^R \mathrm{d}r \sin\big(\pi\xi\cdot\theta r/L\big) = \frac{L}{\pi(\xi\cdot\theta)}\Big[\cos\big(\pi\xi\cdot\theta R/L\big) - 1\Big] = -\frac{2L}{\pi(\xi\cdot\theta)} \sin^2\big(\pi\xi\cdot\theta R/(2L)\big). \tag{49}$$

Hence,

$$G(\xi,\chi) = -\int_{S^1} \mathrm{d}\theta \int_{S^1} \mathrm{d}\theta'\, \mathscr{P}\big(1/(\theta\cdot\theta')\big) \phi_R(\xi\cdot\theta)\phi_R(\chi\cdot\theta'). \tag{50}$$

We approximate G using numerical quadrature with a trapezoidal rule. To deal with the singularity in the principal value integral, we take the grids of θ and θ' to be

$$\theta_j = \exp(i(j-1)\pi/J), \quad \text{and} \quad \theta'_j = \exp(i(j-1/2)\pi/J), \qquad j = 1,\ldots,J \tag{51}$$

for some positive integer J. The quadrature rule converges exponentially [17, Section 6]. Due to symmetry, only quadrature points on half circles are required. We arrive at the final approximation

$$G(\xi,\chi)\approx\sum_{j=1}^{J}\sum_{j'=1}^{J}\omega_{G,j,j'}\phi_{R,j}(\xi)\phi'_{R,j'}(\chi) \tag{52}$$

where the weights are given by

$$\omega_{G,j,j'}=-\Big(\frac{2\pi}{J}\Big)^2\frac{1}{\theta_j\cdot\theta'_{j'}} \tag{53}$$

and we have used the shorthand notation

$$\phi_{R,j}(\xi)=\phi_R(\xi\cdot\theta_j)\quad\text{and}\quad\phi'_{R,j'}(\chi)=\phi_R(\chi\cdot\theta'_{j'}). \tag{54}$$

In summary, we have obtained the approximation

$$\begin{aligned}\widehat{I}_1(\xi)&\approx\sum_{\substack{\chi,\eta,\zeta,\\ \chi+\eta+\zeta=\xi}}\sum_{j,j'}\omega_{G,j,j'}\,\widehat{f}(\chi)\,\widehat{g}(\eta)\,\widehat{h}(\zeta)\,\phi_{R,j}(\chi+\eta)\,\phi'_{R,j'}(\eta)\\&=\sum_{j,j'}\omega_{G,j,j'}\sum_{\zeta}\Big[\sum_{\eta}\widehat{f}(\xi-\zeta-\eta)\,\big(\phi'_{R,j'}(\eta)\,\widehat{g}(\eta)\big)\Big]\phi_{R,j}(\xi-\zeta)\,\widehat{h}(\zeta).\end{aligned} \tag{55}$$

For each j and j', we first calculate the product $\phi'_{R,j'}\widehat{g}$ (complexity $\mathcal{O}(JN^2)$); the summation over η is a convolution by FFT ($\mathcal{O}(JN^2\log N)$); we then multiply the result pointwise with $\phi_{R,j}$ ($\mathcal{O}(J^2N^2)$). The summation over ζ is another convolution ($\mathcal{O}(J^2N^2\log N)$). The total complexity is thus $\mathcal{O}(J^2N^2\log N)$. We use double zero padding in the Fourier coefficients to avoid aliasing.

The dissipative part (40) in Carleman representation reads

$$\begin{aligned}\mathscr{C}_{\mathrm{d}}[W](v)=\pi\int_{B_R}\int_{B_R}\mathrm{d}u\,\mathrm{d}u'\,\delta(u\cdot u')\Big(&2\big\langle w(v+u),w(v+u')\big\rangle_{\eta}\big(\mathbb{1}-W(v)-(\eta w(v+u+u'))\cdot\boldsymbol{\sigma}\big)\\&+(2w_0(u+v)-1)\big\{W(v),(\eta w(v+u+u'))\cdot\boldsymbol{\sigma}\big\}\Big),\end{aligned} \tag{56}$$

which follows from (40) by the same change of variables leading to (41). Expanding the above expression, it is straightforward to check that it consists of the following three kinds of integrals:

$$I_2(v)=\int_{B_R}\int_{B_R}\mathrm{d}u\,\mathrm{d}u'\delta(u\cdot u')f(v+u)g(v+u')h(v); \tag{57}$$

$$I_3(v)=\int_{B_R}\int_{B_R}\mathrm{d}u\,\mathrm{d}u'\delta(u\cdot u')f(v+u)g(v+u')h(v+u+u'); \tag{58}$$

$$I_4(v)=\int_{B_R}\int_{B_R}\mathrm{d}u\,\mathrm{d}u'\delta(u\cdot u')f(v+u)g(v+u+u')h(v), \tag{59}$$

where f,g,h stand for certain components of w. To evaluate these integrals, we define

$$H(\xi,\chi)=\int_{B_R}\mathrm{d}u\int_{B_R}\mathrm{d}u'\,\delta(u\cdot u')\exp(i\pi\xi\cdot u/L)\exp(i\pi\chi\cdot u'/L). \tag{60}$$

By similar steps as leading to (52), one obtains

$$H(\xi,\chi)\approx\sum_{j=1}^{J}\omega_{H,j}\,\psi_{R,j}(\xi)\,\psi'_{R,j}(\chi). \tag{61}$$

Here

$$\omega_{H,j}=\frac{\pi}{J},\quad\psi_{R,j}(\xi)=\frac{2L}{\pi\xi\cdot\theta_j}\sin\Big(\frac{\pi R}{L}\xi\cdot\theta_j\Big)\quad\text{and}\quad\psi'_{R,j}(\chi)=\frac{2L}{\pi\xi\cdot\theta_j}\sin\Big(\frac{\pi R}{L}\xi\cdot\mathscr{R}_{\pi/2}\theta_j\Big), \tag{62}$$

where $\mathscr{R}_{\pi/2}$ is the rotation by $\pi/2$.

Then the Fourier representation of I_2 is

$$\begin{aligned}\widehat{I_2}(\xi) &= \sum_{\substack{\chi,\eta,\zeta,\\ \chi+\eta+\zeta=\xi}} \sum_j \omega_{G,j} \widehat{f}(\chi)\,\widehat{g}(\eta)\,\widehat{h}(\zeta)\,\psi_{R,j}(\chi)\,\tilde{\psi}_{R,j}(\eta) \\ &= \sum_j \omega_{G,j} \sum_\zeta \sum_{\chi+\eta=\xi-\zeta} \big(\psi_{R,j}(\chi)\,\widehat{f}(\chi)\big)\big(\tilde{\psi}_{R,j}(\eta)\,\widehat{g}(\eta)\big)\,\widehat{h}(\zeta). \end{aligned} \tag{63}$$

For each j, the pointwise products in the brackets are computed (complexity $\mathcal{O}(JN^2)$); for each j and ξ, summation over χ, η and ζ is a double convolution by FFT ($\mathcal{O}(JN^2 \log N)$). The total complexity is ($\mathcal{O}(JN^2 \log N)$). The integral type I_4 is similar to I_1, and hence we will omit the details.

For I_3, we need another representation of $H(\xi, \chi)$, as suggested by Hu and Ying in [7]:

$$\begin{aligned} H(\xi,\chi) &\approx \frac{\pi}{J} \sum_{m=1}^{M} w_{R,m} \sum_{j=1}^{J} \Big[\exp(i\pi\rho_{R,m}\xi\cdot\theta_j/L)\,\psi'_{R,j}(\chi)\Big], \\ &=: \sum_{m=1}^{M}\sum_{j=1}^{J} \tilde{\omega}_{H,j,m}\Big[\exp(i\alpha_{j,m}\cdot\xi)\,\psi'_{R,j}(\chi)\Big] \end{aligned} \tag{64}$$

with

$$\tilde{\omega}_{H,j,m} = \frac{\pi}{J} w_{R,m} \quad \text{and} \quad \alpha_{j,m} = \pi\rho_{R,m}\theta_j/L. \tag{65}$$

In the above, $(\rho_{R,m}, w_{R,m})$ are the nodes and weights of a Gauss–Legendre quadrature on $[-R, R]$. Then, the integral I_3 can be calculated as

$$\begin{aligned}\widehat{I_3}(\xi) &= \sum_{j,m} \tilde{\omega}_{H,j,m} \sum_{\chi,\eta,\zeta:\,\chi+\eta+\zeta=\xi} \widehat{f}(\chi)\,\widehat{g}(\eta)\,\widehat{h}(\zeta)\,\exp(i\alpha_{j,m}\cdot\chi)\,\exp(i\alpha_{j,m}\cdot\zeta)\,\psi'_{R,j}(\eta+\zeta) \\ &= \sum_{j,m} \tilde{\omega}_{H,j,m} \sum_{\chi,\eta,\zeta:\,\chi+\eta+\zeta=\xi} \big(\exp(i\alpha_{j,m}\cdot\chi)\widehat{f}(\chi)\big)\,\widehat{g}(\eta)\,\psi'_{R,j}(\xi-\chi)\,\big(\exp(i\alpha_{j,m}\cdot\zeta)\,\widehat{h}(\zeta)\big) \\ &= \sum_{j,m} \tilde{\omega}_{H,j,m} \sum_{\chi} \big(\exp(i\alpha_{j,m}\cdot\chi)\,\widehat{f}(\chi)\big)\,\psi'_{R,j}(\xi-\chi) \sum_{\eta,\zeta:\,\eta+\zeta=\xi-\chi} \widehat{g}(\eta)\,\big(\exp(i\alpha_{j,m}\cdot\zeta)\,\widehat{h}(\zeta)\big). \end{aligned} \tag{66}$$

We first calculate the pointwise products in the bracket for each j and m ($\mathcal{O}(JMN^2)$); summation over χ, η and ζ is a double convolution ($\mathcal{O}(JMN^2 \log N)$). Since M is $\mathcal{O}(N)$, the total complexity is ($\mathcal{O}(JN^3 \log N)$).

We remark that while the above discussion is limited to the case of two dimensional velocity space, it is possible to extend the method to $3D$ by generalizing the method in [7] to our case. We will leave this to future works. The numerical results in this work are limited to one space dimension and two velocity dimensions.

4. Time splitting algorithm and parallelization

The numerical discretization of Eq. (1) is based on a time splitting algorithm to deal with the convection, collision and external magnetic terms separately. Specifically, we perform half a time step of convection in physical velocity space, then transform the Wigner state to velocity Fourier space using FFT for the collision integrals as discussed in Section 3.2 and for applying the external magnetic field, and finally switch back to physical velocity space for another half time step of convection. For the convection we use the finite volume method with minmod slope limiter [8, Ch. 16]; other slope limiters can also be applied. For completeness, we briefly recall the formulation with some comments on parallelization of the algorithm.

In the advection step, each discrete velocity v can be treated independently due to the time splitting. The minmod slope limiter method updates the solution as

$$\begin{aligned} W_j^{n+1} = W_j^n + \frac{\Delta t}{2\Delta x}\Big[&-v_x\big(W_{j+1}^n - W_{j-1}^n\big) + |v_x|\big(W_{j+1}^n - 2W_j^n + W_{j-1}^n\big) \\ &+\tfrac{1}{2}\left(\operatorname{sgn}(\hat{v}) - \hat{v}\right)\Big(-v_x\big(S_{j+1}^n - S_{j-1}^n\big) + |v_x|\big(S_{j+1}^n - 2S_j^n + S_{j-1}^n\big)\Big)\Big], \end{aligned} \tag{67}$$

where Δx denotes the spatial mesh width, Δt the time step, n the discretized time index, j the finite volume cell index, and $\hat{v} = \Delta t\, v_x/\Delta x$. We use the shorthand notations

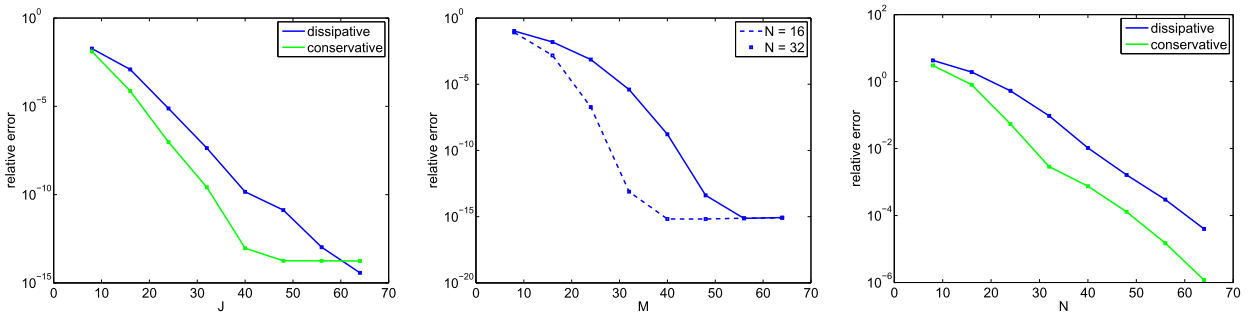

(a) convergence with J (b) convergence with M (c) convergence with N

Fig. 1. Exponential convergence of the dissipative $\mathscr{C}_\mathrm{d}$ and conservative $\mathscr{C}_\mathrm{c}$ collision operator calculation with respect to J, M and N, for fixed domain size parameter $L = 12$ and truncation radius $R = 7.5$. The collision operators are applied to the Wigner state in (69) and compared to a reference calculation with $J, M, N = 72$, respectively. The relative error is calculated using the L^1-norm of the representation as $N \times N$ matrices in Fourier grid space. In (a) we have additionally fixed $N = M = 32$, in (b) $J = 32$ and in (c) $J = 32$, $M = 72$.

$$W_j^n = W(n\,\Delta t, j\,\Delta x, v) \quad \text{and} \quad S_j^n = \operatorname{minmod}\left(W_{j+1}^n - W_j^n, W_j^n - W_{j-1}^n\right)$$

with the minmod function defined as

$$\operatorname{minmod}(a,b) = \begin{cases} a & \text{if } |a| \le |b| \text{ and } a\,b > 0; \\ b & \text{if } |b| < |a| \text{ and } a\,b > 0; \\ 0 & \text{if } a\,b < 0. \end{cases} \tag{68}$$

The first line in Eq. (67) is precisely Godunov's method, and the second line originates from the additional slope limiter terms. As mentioned above, for the time splitting algorithm we actually perform two transport steps with $\Delta t/2$. Note that the Wigner state at the next time step depends on *two* neighbors on either side, i.e., on the five finite volumes with indices $j-2, \ldots, j+2$.

Concerning parallelization, each computing node handles a few adjacent finite volumes, that is, we parallelize the computation along the spatial x dimension. This straightforward approach takes advantage of the locality of the computationally demanding collision step, which is independent of the neighboring finite volumes. Since the transport step (67) depends on two neighbors on each side, every computing node handles at least two adjacent finite volumes to minimize inter-process communication. In our custom C implementation, we use MPI to transfer neighboring states during the transport step.

5. Numerical examples

5.1. Validation of the algorithm

We first present several numerical tests to validate our algorithm. Let us start with the approximation of the kernels G in (52) and H in (61) and (64), which depend on the choice of the number $2J$ of points on the unit circle in (51), and the total number M of Gauss–Legendre quadrature nodes on $[-R, R]$ for the radial quadrature in (64). To test the dependence on these parameters, we calculate the dissipative and conservative collision kernels $\mathscr{C}_\mathrm{d}[W]$ and $\mathscr{C}_\mathrm{c}[W]$ for a fixed spin density matrix $W(v)$. Here, $W(v)$ is (somewhat arbitrarily) chosen as

$$\begin{aligned} W(v) = {} & \frac{1}{3\pi}(1+v_x)\mathrm{e}^{-\frac{1}{2}(v_x-1/2)^2-\frac{1}{2}(v_y+v_x)^2}\mathbb{1} + \frac{3\sqrt{6/5}}{55\pi}\left(1 - v_x - \tfrac{v_y}{6}\right)^2 \mathrm{e}^{-\frac{1}{12}(2v_x+v_y)^2-\frac{1}{10}v_y^2}\sigma_1 \\ & + \frac{1}{4\pi\sqrt{2}}\mathrm{e}^{-\frac{1}{8}(v_x-1)^2-\frac{1}{4}v_y^2}\sigma_2 + \frac{9}{56\pi}\left(\tfrac{1}{3}+v_x\right)^2 \mathrm{e}^{-\frac{1}{8}(v_x-v_y)^2-\frac{1}{8}(v_x+2v_y)^2}\sigma_3\,. \end{aligned} \tag{69}$$

The Fourier representation determines the discretization in physical velocity space, i.e., $v \in (2L/N)\,\Xi$ with N the number of Fourier grid points in each dimension, Ξ the corresponding grid defined in (43) and L the domain size.

First we change J while keeping the other parameters fixed, and compare the result to a reference calculation with large $J = 72$. The relative error is calculated as $\sum_{j=0}^3 \|\mathscr{C}_\mathrm{d}[W]_j - \mathscr{C}_{\mathrm{d,ref}}[W]_j\| / \|\mathscr{C}_{\mathrm{d,ref}}[W]_j\|$ (and correspondingly for $\mathscr{C}_\mathrm{c}$), where j denotes the Pauli matrix component as in (30) and $\|\cdot\|$ is the L^1-norm of the representation as $N \times N$ matrices in Fourier grid space. One observes in Fig. 1(a) that the relative error decreases exponentially fast as J increases, confirming the previous discussion of exponential convergence with respect to J. Fig. 1(a) also illustrates that $J = 32$ already achieves relative errors smaller than 10^{-8} (note that $J = 32$ amounts to 64 grid points in θ due to symmetry). We will fix this choice in the sequel.

Next, we study the accuracy of the approximation (64) for different choices of M. As discussed before, the integrand becomes more oscillatory as N increases, and thus we expect that the number of quadrature nodes M depends linearly on N.

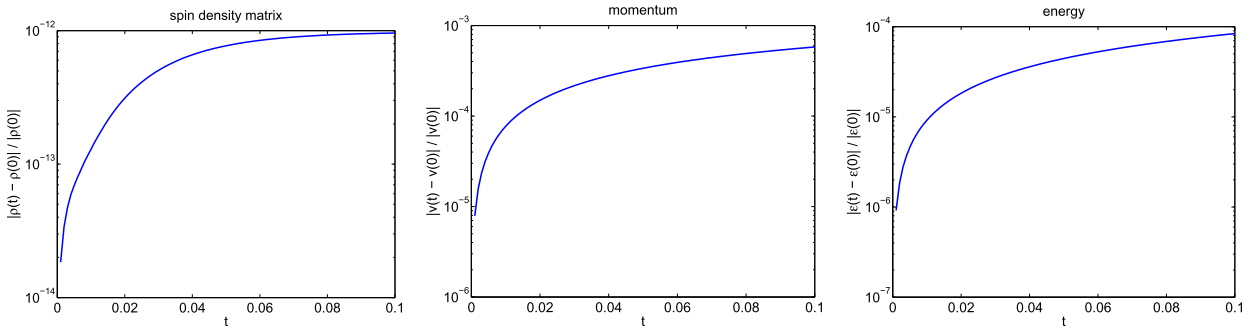

(a) spin density matrix (b) momentum (c) energy

Fig. 2. Conservation of the spin density (12), momentum (13) and energy (14) by the numerical scheme for the spatially homogeneous setting with parameters $N = 32$, $L = 12$, $J = 32$, $M = 32$, $R = 7.5$, initial state (70) and time step $\Delta t = 0.001$. The y-axis shows the relative deviation from the initial value on a logarithmic scale.

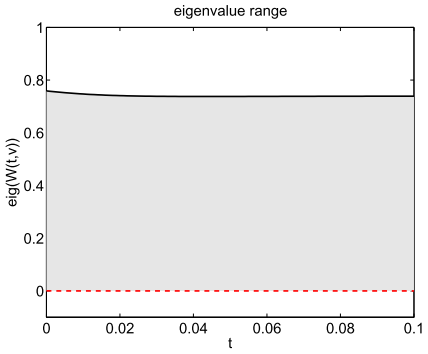

Fig. 3. Time-dependent range of the eigenvalues of the Wigner states, remaining between 0 and 1, as required (same simulation as in Fig. 2).

The relative error of the dissipative $\mathscr{C}_{\mathrm{d}}[W]$ collision term also seems to decay exponentially with M before reaching the machine accuracy (see Fig. 1(b)), thanks to the accuracy of the Gauss–Legendre quadrature. In our subsequent computations we fix $M = 32$, which is adequate to achieve 10^{-5} relative error for $N = 32$.

Finally, the exponential convergence with respect to N in Fig. 1(c) verifies that our method achieves spectral accuracy in dealing with the collision operators. A large $M = 72$ is used in Fig. 1(c) to ensure the accuracy of the approximation (64) for each N.

5.2. Spatially homogeneous equation

We now study the time evolution under the spatially *homogeneous* equation. Here we choose the initial condition to be a Fermi–Dirac state perturbed by v-dependent rotations:

$$W(0, v) = \mathrm{e}^{-iX(v)} \cdot U_0 \cdot \mathrm{diag}\big(\mathrm{e}^{\left(\frac{1}{2}|v-v_0|^2-\mu_s\right)/(k_{\mathrm{B}}T)} + 1\big)_s^{-1} \cdot U_0^* \cdot \mathrm{e}^{iX(v)} \tag{70}$$

with

$$U_0 = \begin{pmatrix} \cos(\pi/5) & -i\sin(\pi/5) \\ \sin(\pi/5) & i\cos(\pi/5) \end{pmatrix}, \quad X(v) = \sin\left(v_y^2\right)\mathbb{1} + (v_x - 1)\sigma_1 + 2\left(v_x^2 + |v_y| + 1\right)^{-1}\sigma_2 + \cos\left(v_x + \tfrac{1}{2}v_y\right)\sigma_3$$

and the parameters $k_{\mathrm{B}}T = 5/4$, $\mu_\uparrow = 1$, $\mu_\downarrow = 3/2$ and $v_0 = (0.4, -0.1)$. In Fig. 2, the conserved quantities spin density (12), momentum (13) and energy (14) are plotted as a function of time. We use the matrix L^2-norm for the relative error of the 2×2 spin density $\rho(t)$. Excellent conservation is observed numerically (note that the scale of the y-axes are 10^{-12}, 10^{-4} and 10^{-5} respectively). We have used the time step $\Delta t = 0.001$ for the simulation. As another consistency check, the eigenvalues of the Wigner spin-density matrices must stay between 0 and 1. This condition is satisfied by our numerical scheme: Fig. 3 visualizes the largest and smallest (with respect to v) of all eigenvalues. In accordance with the H-theorem, the entropy is monotonically increasing (see Fig. 4(a)). Physically, as $t \to \infty$ the Wigner state should converge to a thermal equilibrium Fermi–Dirac distribution W_{FD} (17) with moments (18) matching the conserved moments of the Wigner state (see Fig. 2). The average velocity u leads to a shift $W_{\mathrm{FD}}(v) \to W_{\mathrm{FD}}(v - u)$ in (17), and the eigenbasis of W_{FD} is equal to the eigenbasis of the spin density matrix ρ. We fit the temperature T and chemical potentials $\mu_\uparrow$, $\mu_\downarrow$ in (18) numerically to

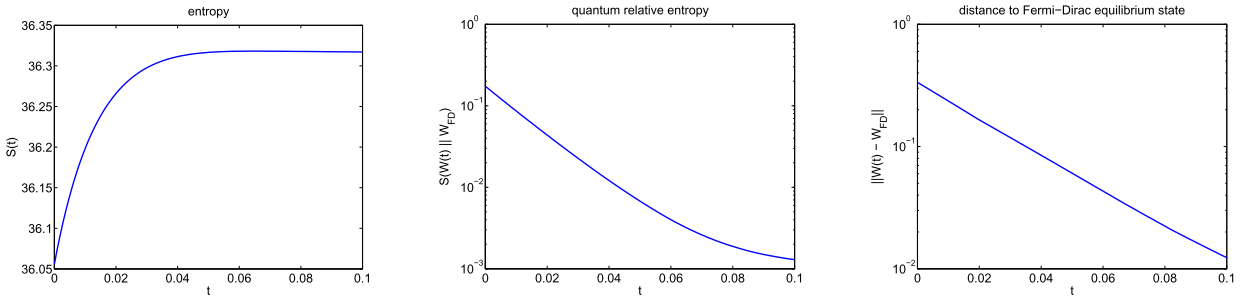

(a) entropy (b) quantum relative entropy (c) convergence to W_{FD}

Fig. 4. Time-dependent entropy (a) and quantum relative entropy (b) as specified in Eq. (71), as well as the L^1-norm distance (c) to the asymptotic Fermi–Dirac equilibrium state determined by the conservation laws (spatially homogeneous case, same simulation as in Fig. 2).

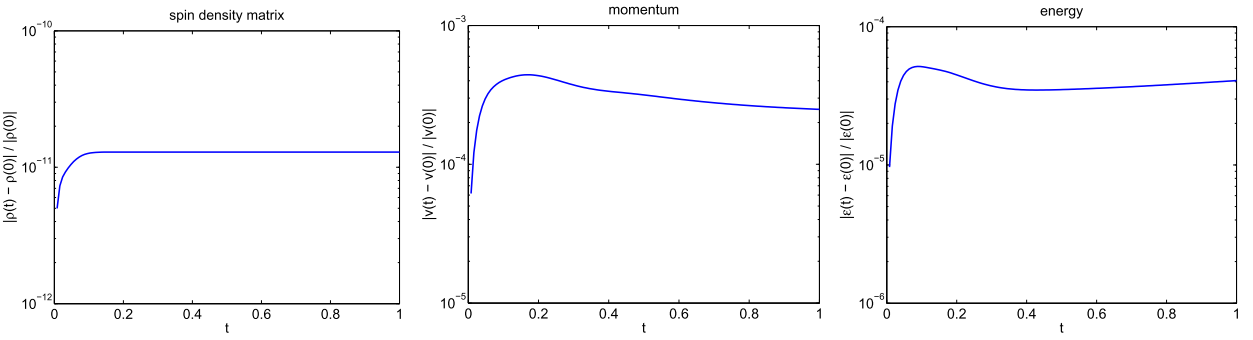

(a) spin density matrix (b) momentum (c) energy

Fig. 5. Conservation of the (spatially averaged) spin density (12), momentum (13) and energy (14) by the numerical scheme for the spatially inhomogeneous equation with periodic boundary conditions and $x \in [0, 1)$. The parameters in this simulation are $N = 32$, $L = 12$, $J = 32$, $M = 32$, $R = 7.5$, the mesh width $\Delta x = 0.1$ and the time step $\Delta t = 0.008$.

match the eigenvalues of ρ and the energy. The expected convergence to W_{FD} is verified in Fig. 4(b), showing the quantum relative entropy between the Wigner state and W_{FD}. The quantum relative entropy is given by (recall that $\tilde{W} = \mathbb{1} - W$)

$$S(W \parallel W_{\mathrm{FD}}) = \int \mathrm{tr}\Big[W(v)\big(\log W(v) - \log W_{\mathrm{FD}}(v)\big) + \tilde{W}(v)\big(\log \tilde{W}(v) - \log \tilde{W}_{\mathrm{FD}}(v)\big)\Big]\,\mathrm{d}v. \tag{71}$$

Using the H-theorem for the entropy and the conservation property of the fluid dynamic moments, the relative entropy is monotonically decaying to zero as $t \to \infty$. Finally, we demonstrate exponential convergence to W_{FD} in L^1-norm in Fig. 4(c).

5.3. Spatially inhomogeneous equation with periodic boundary conditions

For *periodic* boundary conditions, the spin density, momentum, and energy are still conserved globally, i.e., after taking the integral over the spatial dimension. Fig. 5 shows the conservation in the numerical scheme, analogous to the spatially homogeneous case. The initial Wigner state is similar to (70) but with T, μ_s and v_0 depending on the spatial location x.

The quantum relative entropy now involves integration over the spatial domain:

$$S\big(W(t,\cdot,\cdot) \parallel W_{\mathrm{FD}}\big) = \int S\big(W(t,x,\cdot) \parallel W_{\mathrm{FD}}\big)\,\mathrm{d}x. \tag{72}$$

Note that the asymptotic Fermi–Dirac equilibrium state is independent of t and x. For comparison, we define a quantum relative entropy with respect to locally fitted (at each x and t) Fermi–Dirac states:

$$S_{\mathrm{loc}}\big(W(t,\cdot,\cdot) \parallel W_{\mathrm{FD,loc}}(t,\cdot,\cdot)\big) = \int S\big(W(t,x,\cdot) \parallel W_{\mathrm{FD,loc}}(t,x,\cdot)\big)\,\mathrm{d}x. \tag{73}$$

Here $W_{\mathrm{FD,loc}}(t,x,\cdot)$ is the Fermi–Dirac state with the same spin density, momentum and energy as $W(t,x,\cdot)$. Fig. 6(a) visualizes the monotonically increasing entropy, and Fig. 6(b) visualizes the quantum relative entropy, both global and local (for the same simulation as in Fig. 5). It is straightforward to verify that

$$S\big(W(t) \parallel W_{\mathrm{FD}}\big) = S\big(W(t) \parallel W_{\mathrm{FD,loc}}(t)\big) + S\big(W_{\mathrm{FD,loc}}(t) \parallel W_{\mathrm{FD}}\big). \tag{74}$$

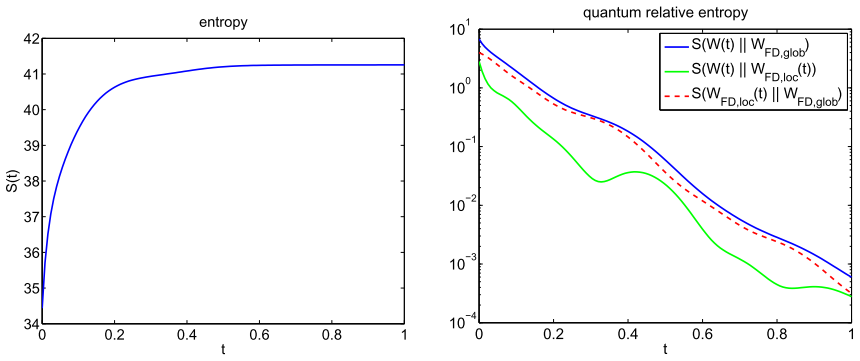

(a) entropy (b) quantum relative entropy

Fig. 6. Time-dependent entropy (a) and quantum relative entropy (b) for the spatially inhomogeneous equation with periodic boundary conditions and $x \in [0, 1)$. In (b), the blue curve shows the entropy relative to the global, uniform Fermi–Dirac state (Eq. (72)), whereas the green curve displays the entropy relative to locally fitted (at each x and t) Fermi–Dirac states (Eq. (73)). (For interpretation of the references to color in this figure legend, the reader is referred to the web version of this article.)

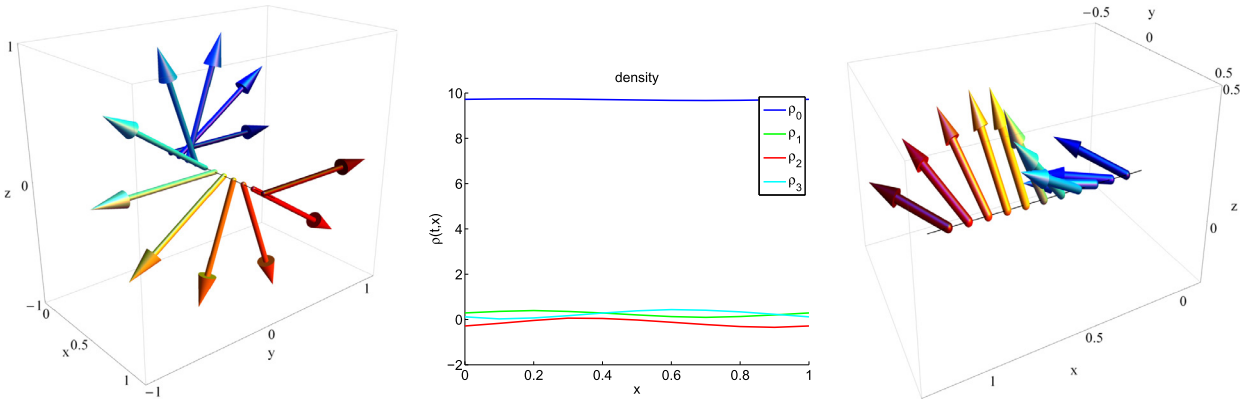

(a) external magnetic field (b) density $\rho(t, x)$ at $t = 1$ (c) $\frac{1}{2}$ Bloch vector of density

Fig. 7. (a) Visualization of the external magnetic field in Eq. (75), with color encoding the position along the x axis. (b) Components of the corresponding spin density matrix $\rho(t, x)$ in the Pauli representation (30) for a simulation with this magnetic field, periodic boundary conditions and finite volume size $\Delta x = 0.1$. (c) Visualization of the corresponding Bloch vector part of the density (for clarity, the axis is rotated compared to (a)). (For interpretation of the references to color in this figure legend, the reader is referred to the web version of this article.)

According to Fig. 6(b), the quantum relative entropy is dominated by $S\big(W_{\mathrm{FD,loc}}(t) \parallel W_{\mathrm{FD}}\big)$. In other words, the system quickly relaxes to a local Fermi–Dirac state, before converging to the global equilibrium.

As next step, we investigate the effect of an external, x-dependent magnetic field, which enters the Boltzmann equation as the last term in Eq. (1). Specifically, we choose

$$\vec{B}(x) = (0, \cos(2\pi x), \sin(2\pi x))^T \tag{75}$$

for the simulation. Fig. 7 visualizes the external magnetic field and shows the components of the spin density matrix at $t = 1$, with the Bloch vector part (scaled by $\frac{1}{2}$) defined as $\vec{\rho} = (\rho_1, \rho_2, \rho_3)$. Compared to the above simulation without magnetic field (density not shown), the Bloch vector components of $\rho(t, x)$ now change with x. Since the magnetic field acts as a unitary rotation of the Wigner state in the time evolution, the trace $\mathrm{tr}[W(t, x, v)]$ remains unaffected by the magnetic field and the momentum and energy conservation laws still hold.

5.4. *Spatially inhomogeneous equation with Dirichlet and Maxwell boundary conditions*

First, we investigate a simulation with Dirichlet boundary conditions. The fixed states at the left and right boundary are Fermi–Dirac states (17) with different temperatures and eigenbasis, as summarized in Table 1. Here, U contains the spin-eigenbasis of the Fermi–Dirac state as column vectors. In Fig. 8 we visualize the stationary density (after running the simulation until reaching stationarity) as well as the local temperature and entropy. The temperature is estimated by constructing a local Fermi–Dirac state with the same moments as the actual local Wigner state. Note that the stationary temperature at the boundary is not exactly equal to the values in Table 1 since the Dirichlet boundary condition fixes only the incoming parts of the Wigner states at the left and right boundary.

Table 1
Temperature T, chemical potentials $\mu_\uparrow$, $\mu_\downarrow$ and eigenbasis U of the incoming left and right Fermi–Dirac boundary states for a simulation with Dirichlet boundary conditions.

	left	right
$1/(k_\mathrm{B}T)$	0.8	1.2
$\mu_\uparrow$	1.5	1.5
$\mu_\downarrow$	-1.5	-1.5
U	$\mathbb{1}$	$\frac{1}{\sqrt{2}}\begin{pmatrix}1 & -1\\ 1 & 1\end{pmatrix}$

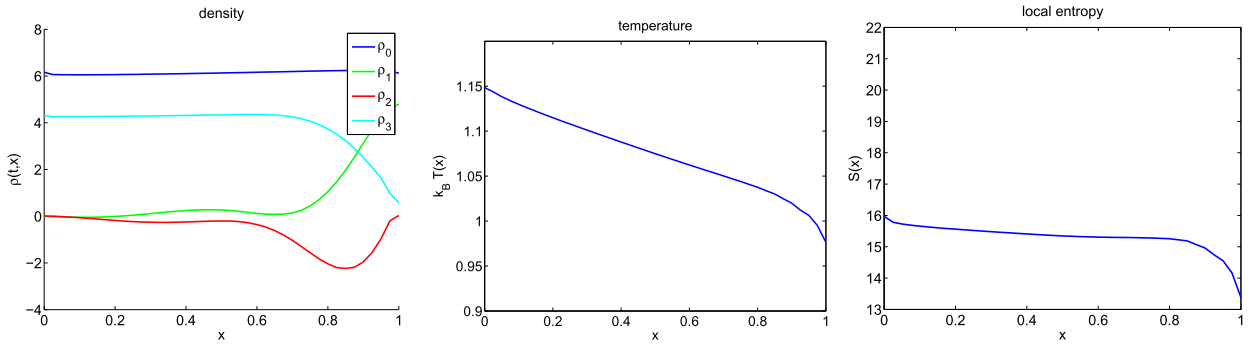

(a) stationary density (b) $k_\mathrm{B}T$ (c) local entropy

Fig. 8. Components of the stationary spin density matrix (a) in the Pauli representation (30), local temperature (b) and local entropy (c) for a simulation with Dirichlet boundary conditions, with finite volume size $\Delta x = 0.025$.

Table 2
Temperature T, chemical potentials $\mu_\uparrow$, $\mu_\downarrow$ and eigenbasis U of the left and right diffusive reflection Fermi–Dirac states for two simulations with Maxwell boundary conditions.

	$1/(k_\mathrm{B}T)$		$\mu_\uparrow$		$\mu_\downarrow$		U	
	left	right	left	right	left	right	left	right
Maxwell (i)	0.6	1.1	-0.4	1.3	1.8	-0.9	$\mathbb{1}$	$\mathbb{1}$
Maxwell (ii)	1	1	1.5	1.5	-1.5	-1.5	$\mathbb{1}$	$\frac{1}{\sqrt{2}}\begin{pmatrix}1 & -1\\ 1 & 1\end{pmatrix}$

Finally, we explore the effects of Maxwell boundary states with (i) different temperature and chemical potentials but common spin eigenbasis, and (ii) the same temperature and chemical potentials but spin eigenvectors pointing to different directions, as summarized in Table 2. The corresponding stationary states (after running the simulation up to $t = 4$) are shown in Fig. 9. Somewhat surprisingly, the stationary density for case (i) with standard spin eigenbasis on the left and right contains nonzero off-diagonal entries, see Fig. 9(a). This might result from the interaction of different spin components in the collision operator, such that the local eigenbasis of the stationary state changes with spatial location. Nonzero off-diagonal entries in the stationary spin density are also observed for case (ii) in Fig. 9(d), but here this effect is certainly attributable to the rotated eigenbasis of the right Maxwell boundary condition. The stationary temperature for case (i) smoothly interpolates between the left and right boundary condition (see Fig. 9(b)), as one might expect. The temperature for case (ii) remains constant, in accordance with the same temperature on the left and right (see Fig. 9(e)). Finally, the local entropy tends to decrease with temperature in case (i) and remains largely unaffected by the rotation of the local eigenbasis in case (ii). Recall that the entropy (15) is invariant under a change of eigenbasis. In summary, the local temperature and entropy conform with reasonable expectations, but the local spin eigenbasis of the density $\rho(t, x)$ could have hardly been predicted from the Maxwell boundary conditions.

6. Conclusions and outlook

We have developed an efficient numerical algorithm based on spectral Fourier discretization for the matrix-valued quantum Boltzmann equation. The effective Hamiltonian (6) appears only in the matrix-valued version (since a commutator of scalars vanishes) and consists of a principal value integral lacking microscopic energy conservation; we have introduced a shift in the numerical grid points (51) to treat the singular part of the principal value. The resulting algorithm exhibit spectral accuracy as numerically confirmed in Fig. 1(c).

Our numerical simulations support the picture of fast convergence to local equilibrium and slower global equilibration, see Fig. 6(b). This suggests that future work on effective hydrodynamic equations derived from the matrix-valued quantum Boltzmann equation might be a promising endeavor. A multiscale algorithm coupling the many-body Hubbard model, the

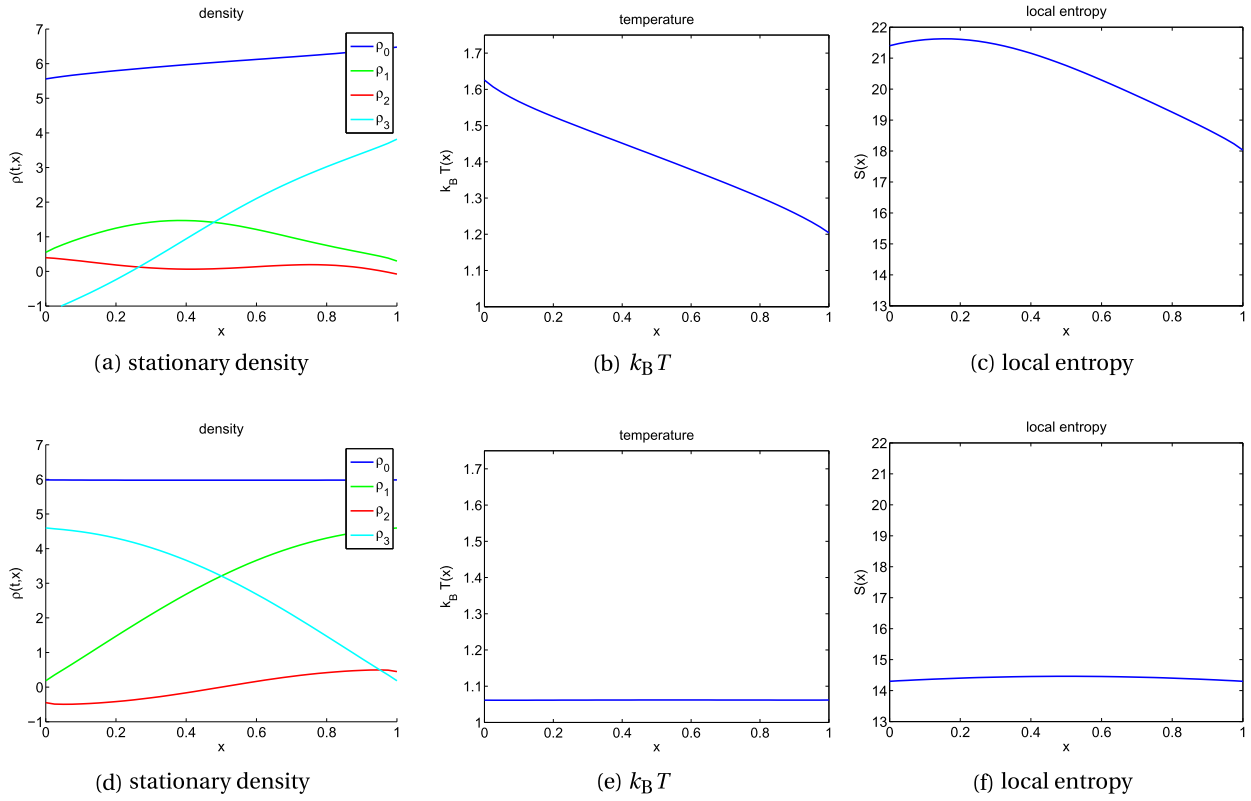

(a) stationary density (b) $k_B T$ (c) local entropy

(d) stationary density (e) $k_B T$ (f) local entropy

Fig. 9. Components of the stationary spin density matrix, local temperature and local entropy for two simulations with Maxwell boundary conditions, with finite volume size $\Delta x = 0.025$ and $\alpha = 0.4$ (accommodation coefficient for the reflection operator). The upper row corresponds to the parameter set (i) in Table 2, and the lower row to (ii).

kinetic description of the weakly interacting Hubbard system, and the hydrodynamic limit of the model would also be an interesting future direction to explore.

References

[1] T. Carleman, Problèmes Mathématiques dans la Théorie Cinétique des Gaz, Almqvist & Wiksell, 1957.
[2] R. El Hajj, Diffusion models for spin transport derived from the spinor Boltzmann equation, Commun. Math. Sci. 12 (2014) 565–592.
[3] F. Filbert, J. Hu, S. Jin, A numerical scheme for the quantum Boltzmann equation with stiff collision terms, ESAIM: Math. Model. Numer. Anal. 46 (2012) 443–463.
[4] M.L. R. Fürst, J. Lukkarinen, P. Mei, H. Spohn, Derivation of a matrix-valued Boltzmann equation for the Hubbard model, J. Phys. A 46 (2013) 485002.
[5] M.L. R. Fürst, C.B. Mendl, H. Spohn, Matrix-valued Boltzmann equation for the Hubbard chain, Phys. Rev. E 86 (2012) 031122.
[6] M.L.R. Fürst, C.B. Mendl, H. Spohn, Matrix-valued Boltzmann equation for the non-integrable Hubbard chain, Phys. Rev. E 88 (2013) 012108.
[7] J. Hu, L. Ying, A fast spectral algorithm for the quantum Boltzmann collision operator, Commun. Math. Sci. 10 (2012) 989–999.
[8] R. LeVeque, Numerical Methods for Conservation Laws, SIAM, 1992.
[9] P.A. Markowich, C. Ringhofer, C. Schmeiser, Semiconductor Equations, Springer-Verlag, New York, 1990.
[10] C.B. Mendl, Matrix-valued quantum lattice Boltzmann method, Int. J. Mod. Phys. C 26 (2015) 1150113.
[11] C. Mouhot, L. Pareschi, Fast algorithms for computing the Boltzmann collision operator, Math. Comput. 75 (2006) 1833–1852.
[12] L.W. Nordheim, On the kinetic method in the new statistics and its application in the electron theory of conductivity, Proc. R. Soc. A 119 (1928) 689–698.
[13] R.E. Peierls, Zur kinetischen Theorie der Wärmeleitung in Kristallen, Ann. Phys. 3 (1929) 1055–1101.
[14] S. Possanner, C. Negulescu, Diffusion limit of a generalized matrix Boltzmann equation for spin-polarized transport, Kinet. Relat. Models 4 (2011) 1159–1191.
[15] D.V. Semikoz, I.I. Tkachev, Kinetics of Bose condensation, Phys. Rev. Lett. 74 (1995) 3093–3097.
[16] H. Spohn, Kinetics of the Bose–Einstein condensation, Physica D 239 (2010) 627–634.
[17] L.N. Trefethen, J.A.C. Weideman, The exponentially convergent trapezoidal rule, SIAM Rev. 56 (2014) 385–458.
[18] E.A. Uehling, Transport phenomena in Einstein–Bose and Fermi–Dirac gases. II, Phys. Rev. 46 (1934) 917–929.
[19] E.A. Uehling, G.E. Uhlenbeck, Transport phenomena in Einstein–Bose and Fermi–Dirac gases. I, Phys. Rev. 43 (1933) 552–561.
[20] B. Vacchini, K. Hornberger, Quantum linear Boltzmann equation, Phys. Rep. 478 (2009) 71–120.
[21] B. Wennberg, Regularity in the Boltzmann equation and the Radon transform, Commun. Partial Differ. Equ. 19 (1994) 2057–2074.
[22] S.A. Wolf, D.D. Awschalom, R.A. Buhrman, J.M. Daughton, S. von Molnár, M.L. Roukes, A.Y. Chtchelkanova, D.M. Treger, Spintronics: a spin-based electronics vision for the future, Science 294 (2001) 1488–1495.